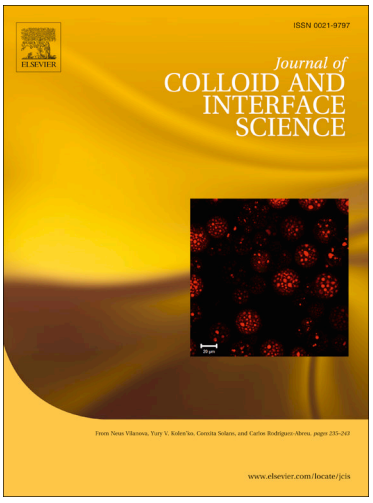

Mechanistic Study of the Nucleation and Conformational Changes of Polyamines in Presence of Phosphate Ions

Patrizia Andreozzi, Caterina Ricci, Joaquin Emiliano Martinez Porcel, Paolo Moretti, Desire De Silvio, Heinz Amenitsch, Maria Grazia Ortore, Sergio Moya

PII: S0021-9797(19)30214-0
DOI: https://doi.org/10.1016/j.jcis.2019.02.040
Reference: YJCIS 24664

To appear in: *Journal of Colloid and Interface Science*

Received Date: 16 November 2018
Revised Date: 9 February 2019
Accepted Date: 11 February 2019

Please cite this article as: P. Andreozzi, C. Ricci, J.E.M. Porcel, P. Moretti, D. De Silvio, H. Amenitsch, M.G. Ortore, S. Moya, Mechanistic Study of the Nucleation and Conformational Changes of Polyamines in Presence of Phosphate Ions, *Journal of Colloid and Interface Science* (2019), doi: https://doi.org/10.1016/j.jcis.2019.02.040

Mechanistic Study of the Nucleation and Conformational Changes of Polyamines in Presence of Phosphate Ions

Patrizia Andreozzi[1], *Caterina Ricci*[2], *Joaquin Emiliano Martinez Porcel*[3], *Paolo Moretti*[2], *Desire De Silvio*[1], *Heinz Amenitsch*[4], *Maria Grazia Ortore*[2*] *and Sergio Moya*[1*]

[1] Soft Matter Nanotechnology Group, CIC biomaGUNE, Paseo Miramón 182 C, 20014 San Sebastián, Guipúzcoa, Spain.

[2] Dipartimento di Scienze della Vita e dell'Ambiente, Università Politecnica delle Marche, Ancona, Italy.

[3] Instituto de Investigaciones Fisicoquímicas Teóricas y Aplicadas (INIFTA), Universidad Nacional de La Plata, Diag 113 y 64, La Plata, Argentina.

[4] Institute of Inorganic Chemistry, Graz University of Technology, Stremayergasse 9/V, Graz, Austria.

*m.g.ortore@univpm.it (M. G. Ortore), *smoya@cicbiomagune.es (S. E. Moya).

Keywords: polyamine phosphate interactions, nanoparticles nucleation, self-assembled nanoparticles, SAXS, DLS.

ABSTRACT

Polyamine Phosphate Nanoparticles (PANs) have great potential for the delivery of large therapeutics, such as plasmids and/or siRNAs. The formation of PANs by complexation of Poly(allylamine hydrochloride) (PAH) and phosphate ions from Phosphate Buffer (PB) was studied here, and how it is affected by the presence of phosphate ions from PB and ionic strength. From Transmission Electron Microscopy (TEM) and Dynamic Light Scattering (DLS) the critical PB concentration for PANs formation was determined. Below this critical point, Small Angle X-ray Scattering (SAXS) studies revealed that small PAH-phosphate aggregates coexist with not complexed or weakly complexed polymer chains in solution and that the presence of the phosphate ions increases the Kuhn length of the polymer chains until that only spherical aggregates are present in solution. TEM, DLS and SAXS showed the increase of PANs size with ionic strength up to 250 mM NaCl. At higher NaCl concentrations, PANs disassemble into smaller aggregates. Isothermal Titration Calorimetry (ITC) showed that PAN formation is an exothermic process and the association of phosphates below the critical PB concentration is entropically controlled.

1. Introduction

Polyamine Phosphate Nanoparticles (PANs) have great potential for the delivery of large therapeutics, such as plasmids and/or siRNAs, which can be complexed to positively charged polyamines through electrostatic interactions [1-3]. PANs are formed by a simple and straightforward one-step procedure, involving the mixing of polyamine solutions and phosphate ions. Their assembly is driven by electrostatic and hydrogen bonding interactions between the positively charged amine groups of the polyamines and the negatively charged phosphate ions. However, a complete description of the molecular mechanisms leading to PANs formation is still missing, to our knowledge.

In a recent paper we have showed that PANs, prepared from poly(allylamine hydrochloride) (PAH) and Phosphate Buffer (PB), are stable at moderate basic pH conditions ($6 \leq$ pH ≤ 9), and disassemble at pHs lower than 6 and higher than 9 [4]. Considering this pH stability, PANs should be stable in the bloodstream and cell media, and then disassemble inside endosomes, following cellular uptake. This response to pH and the capacity that polyamines have for complexing negatively charged molecules makes PANs particularly appealing for use as vectors for drug delivery due to their mechanism of endosomal escape [5-9]. We have shown that siRNAs can be intracellularly delivered with PANs and effectively silence the green fluorescence protein (GFP) [4]. The PB used for PANs fabrication contains sodium hydrogen phosphate (Na_2HPO_4) and potassium dihydrogen phosphate (KH_2PO_4) ions in a molar ratio of 5 to 2, at a buffered pH of 7.6. The ionic strength of the solutions is varied by adding different amounts of NaCl. Monohydrogen and dihydrogen phosphate ions differentiate in their degree of protonation and charge. The monohydrogen phosphate ion, being more negative, can display a stronger interaction with the positively charged amines. On the other hand, the dihydrogen phosphate ion should more easily form hydrogen bonding with the non-protonated amines of PAH. Ionic strength can also play an important role in the association of the polyamine chains, as the charged polymers tend to coil with increasing ionic strength. At low ionic strength, chains are more extended. The state of the chains, extended or coiled, can affect the mechanism of formation of PANs and how the chains are linked among themselves in the presence of the phosphate ions. Additionally, increasing the ionic strength reduces electrostatic repulsion among PAH chains, which can also promote particle growth [10-15].

The aim of this work is to acquire a deeper insight into the interaction of polyamines and phosphate ions, and into the role that the ionic strength plays in the assembly of polyamines into nanoparticles. To achieve this goal, we evaluate the impact of the

phosphate ion concentration and the ionic strength on the formation and growth of PANs using dynamic light scattering (DLS) and transmission electron microscopy (TEM) imaging; two techniques that provide valuable information on the changes in hydrodynamic diameter and size of PANs. We further use isothermal titration calorimetry (ITC) to elucidate the nature of the forces driving to PAN assembly [16, 17]. We perform synchrotron Small Angle X-ray Scattering (SAXS) experiments to investigate the association of polyamines with phosphate ions. SAXS allows us to trace the formation of the PANs at low phosphate concentrations, which are not detectable by DLS, and to study the nucleation process between phosphates and polyamines that leads to the generation of self-assembled nanoparticles. The deeper understanding gained from this work into the mechanism of PANs assembly is a fundamental step toward optimizing these promising candidates as drug delivery vehicles.

2. Experimental Section

2.1. Materials and Chemicals

Poly(allylamine hydrochloride) salt (PAH) (MW: 15 x 10^3 g/mol), phosphate buffer (PB), sodium phosphate dibasic (Na_2HPO_4), potassium phosphate monobasic (KH_2PO_4), hydrochloric acid (HCl), sodium hydroxide (NaOH) and sodium chloride (NaCl) were purchased from Sigma-Aldrich and used as received unless otherwise specified. Polyelectrolyte stock solutions and all subsequent diluted precursor solutions were prepared with MilliQ deionized water. Carbon-coated copper grids and ammonium molybdate were obtained from Electron Microscopy Sciences (USA).

2.2. Preparation of PANs

PANs were prepared in a one-step synthesis by mixing PAH and phosphate salts. PAH (MW ~ 15 kDa) has the following chemical formula $[–CH_2\text{-}CH(CH_2NH_2 * HCl)–]_n$, with an average n ≈ 160. Briefly, 10 μL of a 100 mg/mL (6.7×10^{-3} M) PAH (pH ≈ 4.1) solution were added to 1 mL of Phosphate buffer (PB) in a concentration range between 1÷10 mM (pH ≈ 7.6), to obtain a final PAH concentration of 1 mg/mL (6.7×10^{-5} M). The ionic strength of the solutions was increased by varying the concentration of NaCl from 0 to 350 mM. The same procedure was applied for PAN fabrication with only KH_2PO_4 instead of PB, but at concentrations ranging from 30 to 100 mM (pH ≈ 4.6), and with only Na_2HPO_4, at concentrations from 1 to 10 mM (pH ≈ 9.4). All samples were prepared at room temperature and lefts equilibrate for 10 minutes before to be analyzed. PAN formation was monitored by DLS, measuring the increase of the scattered intensity expressed as derived counts rate. The derived count rate is used to compare the signal strength from different samples. Indeed, the higher derived count rate (kcounts/seconds) usually indicates higher concentration and larger particles. The derived count rate is expressed as measured kcount rate on attenuation factor. The attenuation factor is automatically adjusted by the software to ensure that the scattering intensity is within the optimal range of the Avalanche Photo Diode (APD) detector in the Zetasizer Nano instrument. DLS showed a critical ratio of phosphate and amines below which PAN formation is not detectable due to the low scattering intensities from the samples, which are comparable to the scattered intensity of free PAH in water. The maximum inflection of the scattering curve indicates the minimal molar ratio, R of PB and PAH, $R = ([H_2PO_4^-] \times q^- + [HPO_4^{2-}] \times 2q^-)/([PAH] \times nq^+)$ [4, 5] necessary for formation of PANs that can be detected by DLS.

2.3. Methods

2.3.1. Dynamic light scattering (DLS)

DLS measurements were carried out with a Zeta-Sizer Malvern Instrument in backscattering mode. All experiments were performed at a 173° scattering angle with temperature controlled at 25 °C in 1 mL polystyrene cuvettes. PANs were characterized in terms of size. Short time measurements were carried out for a total of 15 min, with 3 consecutive measurements for each sample.

2.3.2. Transmission electron microscopy (TEM)

2 μL of undiluted PANs prepared from PAH with a concentration of 1 mg/mL and assembled 30 min prior to grid deposition, were transferred to ultra-thin plasma coated carbon film grids and incubated for 1 min. Grids were then washed with degassed Nanopure water, water was removed by applying a paper filter. Then, PANs were incubated with 3 μL of ammonium molybdate 20 mg/mL for 1 min. The excess of staining was also removed by filter paper. Samples were washed three times with degassed Nanopure water. TEM imaging was performed with a JEOL JEM 1010 microscope operating at an acceleration voltage of 100 kV.

2.3.3. Isothermal titration calorimetry (ITC)

ITC experiments were performed with a MicroCalorimeter VP-ITC. Experiments were carried out at 23 °C under continuous stirring of the sample cell at 1000 rpm. 1.456 mL of 1 mg/mL PAH solution was titrated using a stock solution of 0.05 M PB. The titration consisted of 30 injections, the first one of 2 μL PB, and the following ones of 10 μL PB at 150 s intervals each. Data were corrected for the dilution heat of the PB solution. Raw data are reported as a function of the [PB]/[PAH] molar ratio.

2.3.4. Small Angle X-ray Scattering (SAXS)

SAXS experiments were performed at the Elettra Synchrotron, Trieste, Italy [18]. Temperature was kept at 20 °C during measurements. SAXS patterns were recorded using a PILATUS detector. The distance from the sample to the detector was set to 1.5 m to obtain a Q-range from 0.008 to 0.34 $Å^{-1}$. Q is defined as $4\pi\sin\theta/\lambda$, where 2θ is the scattering angle, and $\lambda = 1.5$ Å the X-ray wavelength. We simultaneously recorded the incident and transmitted intensities with the aim of obtaining data on an absolute scale. Hence, normalized SAXS patterns were azimuthally averaged to obtain one-dimensional profiles of scattered intensity. The buffer contribution was subtracted, taking the scattering of the water solutions of phosphate and salts before addition of polyamines as data for the buffer for each condition investigated. Each measurement was performed for 10 s, followed by a dead time of 2 s to avoid radiation damage, and repeated at least 20 times. After checking for radiation damage the data have been averaged.

SAXS data analysis based on the assumption that in each experimental condition flexible disordered polymers can co-exist with spherical nanoparticles. The theoretical fitting on each set of SAXS curves was performed by GENFIT software [19] that takes into account the possible simultaneous presence of non-complexed polymer in solution in the form of worm-like chains (*free*), and polymers entangled in spherical nanoparticles (*PANs*):

$$\frac{d\Sigma}{d\Omega} = x_1 \frac{d\Sigma}{d\Omega}\Big|_{free}(Q) + x_2 \frac{d\Sigma}{d\Omega}\Big|_{PANs}(Q)$$

where x_1 and x_2 account for the fractions of polymer molecules occurring as non-complexed worm-like species, and as polydispersed spheres, respectively. Worm-like species were described according to the theoretical approach for flexible disordered polymers developed by Pedersen-Schurtenberger [20]. In this model the scattering

density takes into account the so called worm-like chain form factor, $P_{PS}(Q)$, multiplied by a two-electron density level cross section for the polymer chain. Hence, for non-complexed *PAH* (*free*) in-solution, the following equation is derived:

$$\left.\frac{d\Sigma}{d\Omega}\right|_{free}(Q) = \frac{cN_A}{M_p} r_e^2 4\pi^2 c_l^2 \left\{ (\rho_p - \rho_s) r_c^2 \frac{J_1(Qr_c)}{Qr_c} + (\rho_S - \rho_0)(r_c + \delta)^2 \frac{J_1[Q(r_c+\delta)]}{Q(r_c+\delta)} \right\}^2 P_{PS}(Q)$$

where N_A is Avogadro's number; r_e is the electron scattering length; r_c the cross-sectional radius of the chain; and c_l the contour length of the chain. The statistical segment b is defined as Kuhn length, represents the separation between two adjacent rigid scattering domains, and it related to the contour length, $c_l = n_b\, b$, and to polymer volume via the cross section radius [21]. The thickness δ and electron density ρ_s of the surrounding shell are also parameters in the model, that we fixed at δ=3 Å (water shell thickness) and at ρ_s=1.05 ρ_0 (water shell density is a little bit higher in respect to bulk water). Solvent electron density ρ_0, polymer concentration c, and molecular weight of the polymer *Mp* are fixed according to experimental data (*c*) and values obtained from literature.[22] The electron density ρ_p is as well a fitting parameter, that we imposed to vary in proximity of literature value [22]. Polymers in solution could be characterized by different rigidity and aggregation features, since they can be found as disordered polymers and polymers entangled in spheres. It is clear that considering single species of non-complexed polymers and just another species of polymer constrained inside the spherical particle is a simplification of the complexity of the system. However, this approach enables us to obtain important information - the average rigidity of the non-complexed polymer in solution and the experimental conditions where just compact

nanoparticles appear- without being obliged to apply wider set of fitting parameters in relation to experimental data. Hence, to corroborate the suitability of our fitting procedure, we performed a global fitting of each set of experimental SAXS data. Common fitting parameters, due to the intrinsic differences in the system, are limited to the electron density ρ_p, and to the worm-like chains cross-section r_c. The parameters that describe the system structure (Kuhn length b, PANs radius R and its polydispersion pD), as well as the weight of the models (x_1 and x_2), are all subjected to a regularization method that avoids dramatic variations or oscillations at increasing ionic strength in solution [23]. This approach, already tested by some of us in previous work [24], allows us to validate our fitting procedure without reducing the system complexity. At lower ionic strength, we imposed to have just disordered polymers, while at higher ionic strength to have just spheres, as confirmed by Kratky plots (see as an example **Fig. 5B**).

3. Results and Discussion

3.1. Characterization of PANs in Phosphate Buffer by DLS, TEM, and ITC.

The driving forces for PAN formation are the electrostatic and hydrogen bonding interactions between the amines of PAH and phosphate ions, as presented in the scheme of **Fig. 1** [15, 26, 27]. The minimal concentration of PB necessary for PAN formation was determined by DLS, measuring the increase of the scattered intensity expressed as derived kilocounts (kcounts). For a constant concentration of 1 mg/mL PAH, the kcounts increase with increasing concentrations of PB until reaching a constant value, as shown in **Fig. 2A**. The maximum inflection of the kcounts curve is observed at 4 mM PB. The inflection indicates the minimal molar ratio of PB necessary for PAN detection by DLS at 1 mg/mL PAH [4]. At 5 mM PB the kcounts value is high, ~10^4. Conversely, the value at 2 mM PB (~ 20 kcounts) was similar to that of the free polymer in water. Indeed, for PB concentrations below 4 mM the scattered intensity remains comparable

to the scattering of PAH in aqueous solution, **Fig. S1**. In order to have an independent estimation of the PB concentration needed for PAN formation, TEM imaging was performed for samples prepared at different PB concentration. TEM images corroborate the results from DLS, **Fig. 2B**: PANs prepared with 2 mM PB show suboptimal structures without clear shapes, indicative of polymer aggregates and probably traces of small nanoparticles with sizes of ~20 nm. At 5 mM PB PANs display a well-defined spherical shape indicative of nanoparticle formation. The hydrodynamic diameter of PANs at 5 mM PB calculated from the intensity distribution from DLS is 86 $\pm$ 34 nm, in good agreement with the size obtained by TEM images show a diameter of 80 $\pm$ 24 nm, hinting that the staining procedure does not affect the size of PANs.

ITC experiments were performed to gain insight into the mechanism of PAN formation. The enthalpy associated with the complexation of polyamines with phosphate ions in PB can lead to a better understanding of the mechanism of PAN formation and of the forces leading to the assembly of PANs, as reported in **Fig. 3** (raw data) *vs* the molar ratio of [PB]/[PAH]. A plot of the binding isotherm of PAH as a function of PB concentration shows three clearly identifiable regions [16, 17], **Fig. 4:** an endothermic region at PB concentrations below 4 mM, suggesting that PANs do not form at these concentrations; an exothermic region at PB concentrations between 4 and 5 mM [27, 28], and a region where the heat progressively decreases to 0 for PB concentrations over 5 mM. An exothermic heat is associated with the concentration of phosphate ions at which nanoparticles start to form, as shown by TEM images and DLS. ITC data hint at the forces involved in the formation of the PANs. At low PB concentrations, the heat released by the complexation of the phosphate with amines is smaller than the heat needed to break the hydrogen bonding of the phosphate and amines with water through their interaction. Since PB associates with the polyamines, we can assume that the association of PAH and phosphate ions at low PB concentration is entropically

controlled [27]. Despite the phosphate ions lose freedom when they associate with PAH chains, the changes in the hydration shell of phosphate ions and amines should lead to more disordered states in water, and consequently to an entropy increase. Although the polymer chains interact with the phosphate ions, they do not completely lose their conformational freedom in bulk at these PB concentrations. Additionally, for each phosphate ion linking two amine groups, at least two Na^+ ions and two Cl^- should be released. As the concentration of PB increases and more amine groups are linked through the phosphate ions, the energetic gain through the complexation of the phosphate ions with the amines overcomes the endothermic changes associated with phosphate/amine dehydration, and the whole processes become exothermic [17]. At high PB concentrations we can assume that there is no more enthalpy gain through the presence of PB as all amines have been linked through the phosphate, or because the organization of the chains in PANs is such that it is not possible to further link amines through phosphate ions. ITC shows that there is already association between phosphate ions and PAH at PB concentrations below 5 mM, which could also be observed by TEM, but not by DLS.

3.1. Characterization of PANs in Phosphate Buffer (PB) by SAXS.

SAXS studies were conducted to have a deeper understanding of the association of PAH and PB at low buffer concentrations,. At PB concentrations below 4 mM, SAXS patterns revealed only the presence of flexible polymers, **Fig. 5A.** Kratky plots, reported in **Fig. 5B**, do not present the characteristic bell shape that indicates the presence of compact objects below 4 mM PB. At PB concentrations higher than 4 mM the Kratky plots do show the presence of compact objects [29]. Therefore, SAXS patterns were fitted by considering the simultaneous presence of flexible non-complexed or disordered polymers, and spheres made out of polymers, as described in detail in the Methods (*2.3.4. Small Angle X-ray Scattering (SAXS)*). The non-complexed polymers

include free polymer in solution, with their counter ions replaced to a certain extend by phosphate ions and some weakly associated chains, which remain soluble in solution. Increasing the concentration of phosphate ions will lead to the further association of these chains into PANs. We will refer to the polymer in solution not forming spherical PANs as non-complexed polymer.

A set of experimental SAXS data, together with their theoretical fitting, are reported in **Fig. 5, 8, 9,** while the overall sets of SAXS data are shown in **Fig. S3**. We note that our unique model is able to describe each series of SAXS experiments, where 1 mg/mL PAH is subjected to increasing concentrations of PB, **Fig. 5A**, and of KH_2PO_4, **Fig. 9A**, and of Na_2HPO_4, **Fig. 9B**. Data clearly demonstrate that at low PB concentrations (< 4 mM) disordered species are predominant. At PB concentrations between 4 and 5 mM disordered polymers and compact spheres can be recognized, as indicated by the fitting parameters reported in **Table S1**. For PB concentrations over 5 mM only spheres are present in solution. The results from the fitting of this set of SAXS curves, confirm DLS and TEM observations, **Fig. 2**. The differences between spheres radii obtained by SAXS and the hydrodynamic radii obtained by DLS can be ascribed to the different properties measured by the two techniques. While DLS measures hydrodynamic diameter, SAXS measures the electronic density of the systems SAXS results clearly show that the Kuhn length increases with increasing PB concentration to reach an approximately constant value (see **Fig. 6**) comparable to the size of the PANs over 5 mM PB. The Kuhn length corresponds to the smallest segment in a polymer that can randomly orient independently of other segments [30, 31]. It is also closely associated with the stiffness of the polymer chains and its value is twice the persistence length. The increase in Kuhn length for increasing PB concentrations below the complete formation of particle spheres, tells us that the polymer becomes stiffer by association with phosphate groups. This finding means that the polymer loses conformational freedom as the concentration

of phosphates increases in solution. Phosphate ions form intra- and inter-chain links with amine groups. Each linking point restricts the mobility of a segment of polymer over lengths that can easily involve several PAH monomers and can be longer than the initial Kuhn length of PAH in bulk, approximately the length of a PAH monomer. The more phosphate ions linking a chain with itself or with other chains, the larger the number of monomers or segments that have a restricted mobility and consequently the longer the Kuhn length. The increase in the Kuhn length is concomitant with the formation of polymer spheres. Once the polymer is only present as spherical particles, then the Kuhn length does not change. It is interesting to notice that there is a sort of critical Kuhn length that is ≈15 nm when compact spheres appear, **Fig. 6**. On the other hand, when 1 mg/mL PAH is subjected to increasing concentrations of PB at a constant ionic strength of 150 mM NaCl, (**Fig. S2** and results in **Table S2**), the screening the charges of PAH results in the critical Kuhn length being smaller at the PB concentration at which spheres are formed.

The Kuhn length (b) is closely associated with the polymer persistence length P, as $P=2b$. P is also related to the bending stiffness by the relation $P=B/(k_BT)$ where k_B is the Boltzmann constant and T the absolute temperature [32, 33]. From our data, we conclude that interaction of phosphates with the poly(allylamine) chains reduces conformational freedom of the chains resulting in stiffer polymers until the formation of particles where the chains are in a precipitated state [30].

3.3. Effect of Ionic Strength

Increasing the ionic strength of the media during PAN preparation has an impact on the size and stability of the nanoparticles. DLS and SAXS measurements show that at low and moderate ionic strengths, up to 250 mM NaCl, the size of the PANs increases with increasing ionic strength, in agreement with previous results (see SAXS fitting

parameters in **Table S3**), **Fig. 7** and **Fig. 8** [4]. However, while the hydrodynamic diameter increases up to 1000 nm at 250 mM NaCl, from SAXS measurements a diameter of less than 28 nm can be determined at the same ionic strength, (inset of **Fig. 8)**. Two possible explanations can be given. First, it could be that a small percentage of large particles in the colloidal suspension can dramatically increase the overall particle diameter derived by DLS, as stated by Tobler et al. [34] A second explanation could be that particles over a certain size are actually the result of the assembly of smaller particles, which are linked among them by phosphate ions. These smaller particles may form, to a large extent through intramolecular association with phosphate ions. Since increasing the ionic strength results in a weakening of the electrostatic repulsion between the particles, they can also associate through phosphate ions but the dense arrangement of PAH, which can be considered as a hard sphere corresponds to the small particles. Evidence supporting this hypothesis can be found in the fact that at ionic strengths higher than 300 mM the particles break into small fragments. Also, at higher ionic strengths, SAXS measurements show that the particles fragment in smaller aggregates as a consequence of the electrostatic shielding of the interaction between phosphates and polyamines. Indeed, at high ionic strength (NaCl $\geq$ 250 mM), SAXS shows that PANs break into disordered polymers and very small nanoparticles, see **Fig. S4**. These results are in agreement with DLS measurements, where both the kcounts and the hydrodynamic size also decrease, **Fig. S5**. Kcounts values at 350 mM NaCl are very similar to the kcounts shown by free-PAH in water. No nanoparticles are detected in solution by DLS. As mentioned above, the instability of PANs at high ionic strength should be related to the screening of charges on the polyamine/phosphate complexes that weakens the interaction between phosphates and polyamines [25, 35].

A complete trend of PAN formation as a function of PB content was obtained in salt-free solution and in 50 mM NaCl by DLS, **Fig. S6** and TEM imaging in **Fig. S7**. In the

presence of 50 mM NaCl, PANs show a larger hydrodynamic diameter, than that obtained in PB without NaCl Figure S6. For 1 mg/mL PAH mixed with 2 mM PB in the presence of 50 mM NaCl, spherical nanoparticles with a diameter of ~30 nm coexist with disordered polymer chains as shown in **Fig. S7A**. Conversely, when 1 mg/mL PAH was mixed with 5 mM PB in the presence of 50 mM NaCl, spherical nanoparticles are formed with a diameter of ~140 nm, **Fig. S7B**. In both conditions the diameter of the spherical nanoparticles is slightly higher than the diameters obtained without NaCl.

3.4 Formation and stability of PANs in Na_2HPO_4 and KH_2PO_4.

The formation of PANs and their stability was further studied by SAXS, DLS, and TEM, for single phosphate components of PB, KH_2PO_4 and Na_2HPO_4. In the presence of only KH_2PO_4, PANs are formed at 50 mM KH_2PO_4, as shown by the change in the shape of SAXS curves, **Fig. 8A** and the hydrodynamic diameters provided by DLS, **Fig. S8A**. SAXS measurements show that, as for PB, the Kuhn length of non-complexed polymers increases with increasing KH_2PO_4 concentration before nanoparticles appear in **Table S4**. Once PANs are formed, their average size also increases as the KH_2PO_4 concentration increases. In the presence of Na_2HPO_4 only, the minimum concentration of phosphate ions necessary for PANs formation was similar to that obtained for PB see **Fig. 8B** and **S8B, Table S5**. From our results, we conclude that PAN formation requires a molar ratio of phosphate to amines $R \cong 11$, in the presence of KH_2PO_4, which is about ten times higher than the ratio of phosphate to amines calculated for Na_2HPO_4 and PB. This is probably due to the fact that to saturate enough positive charges of the polymer and induce PAN formation, more $H_2PO_4^-$ ions are needed. KH_2PO_4 has only one charge, while Na_2HPO_4 has two charges for phosphate ion. PB is mainly formed by HPO_4^{2-}, therefore we expect a similar behavior for PB and Na_2HPO_4. Despite the differences in the minimum concentration of phosphate ions needed for PAN formation, both KH_2PO_4

and Na_2HPO_4 show a similar trend in the evolution of the hydrodynamic diameter with phosphate concentration and ionic strength. Detailed morphological information by TEM of PAN formation in the presence of different phosphate ions and ionic strength is shown in **Fig. S9**. The ionic strength impacts on the formation of PANs with single phosphate components (either KH_2PO_4 or Na_2HPO_4) in a similar way to PAN formation with PB. Indeed, at low phosphate concentration and in the absence of NaCl (20 mM KH_2PO_4, 2 mM Na_2HPO_4) only small PANs, 20 nm in diameter, are formed, which coexist with free polymer in solution (**Fig. S9A** and **C**, upper panel). The same samples prepared with 50 mM NaCl result in larger nanoparticles with diameters of ~ 40 nm, and less free polymer (**Fig. S9E** and **G**, bottom panel). PANs prepared at higher concentrations of phosphate groups (50 mM KH_2PO_4, 5 mM Na_2HPO_4) show a spherical shape and no free polymer can be detected (**Fig. S9B** and **D**, upper panel). Furthermore, the addition of 50 mM NaCl causes a further growth in PAN diameter of ~150 (KH_2PO_4, **Fig. S9F**) and ~300 nm (Na_2HPO_4, **Figure S9H**).

4. Conclusion

Our results provide a deeper understanding of the process of formation of supramolecular PANs and show that there is a decrease in conformational freedom and an increase in stiffness of thepolyamines when these nucleate though amine phosphate interactions. The increase in Kuhn length with increasing PB concentration nicely demonstrates the changes in the state of the polymer from a random walk configuration to a condensed state as PANs form. The ionic strength at which PANs assembly takes place defines the size of the particles, which increases as the ionic strength increases. The increase in particle size with ionic strength can be understood as a result of the screening of repulsive interactions among PAH chains that favors their association. At

ionic strengths over 250 mM, however, the interaction between phosphates and amines is weakened and particles disassembly.

The results of this work advance on the understanding of the self-assembly of polyamine phosphate nanoparticles and the complexation process leading to nanoparticle formation, which to our knowledge has not been tackled before [36, 37]. Future work will focus on the impact on the molecular characteristics of polymer and phosphates on the nucleation and structure of the nanoparticles. We plan to study PAN formation with polyamines of different Mw, and in presence of phosphate salts with larger number of phosphate groups, such as $Na_5P_3O_{10}$, $Na_6P_6O_{18}$, and Sodium polyphosphate (Graham's salt). A more detailed study of the impact of pH on PANs formation is as well planned.

FIGURES

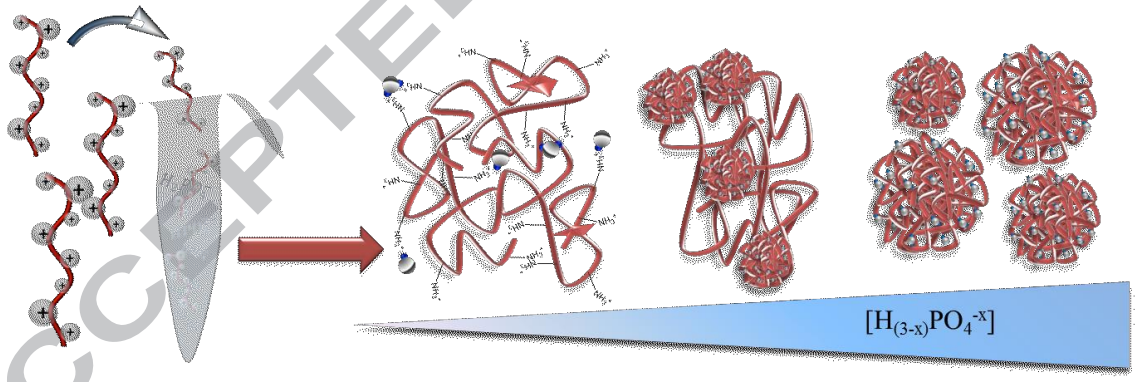

Figure 1. Schematic illustration of PAN preparation in presence of phosphate ions, $[H_{(3-x)}PO_4^{-x}]$. In a standard preparation procedure 10 µL of 100 mg/mL PAH are added to 1 mL of phosphate solution with or without NaCl. In the sketch, single PAH chains are shown linked by the phosphate ions interacting with the amine groups of PAH. The size of the PANs increases as the concentration of $[H_{(3-x)}PO_4^{-x}]$ increases.

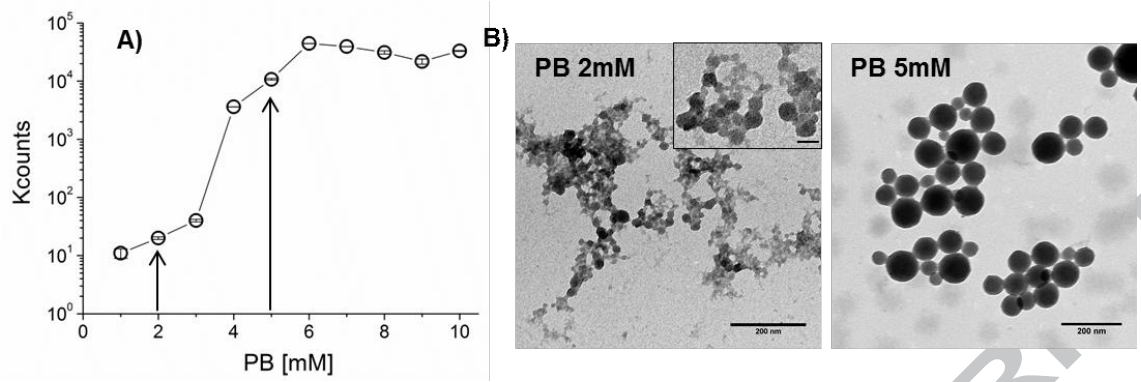

Figure 2. DLS and TEM characterization of PANs formation at constant PAH concentration. A) Derived light scattered intensity (kcounts) of PAH at 1 mg/mL *vs* different concentrations of PB. Results are mean of 3 independent measurements. Error bar are the standard deviation of 3 independent measurements. The line is a guide to the eyes. B) TEM images of PANs synthesized starting from 1 mg/mL PAH in 2 mM PB (left) and PANs synthesized starting from 1 mg/mL PAH in 5 mM PB (right). TEM images correspond to the points in the DLS curve marked with an arrow. Scale bars in the figures indicate 200 nm, while in the inset the bar indicates 50 nm.

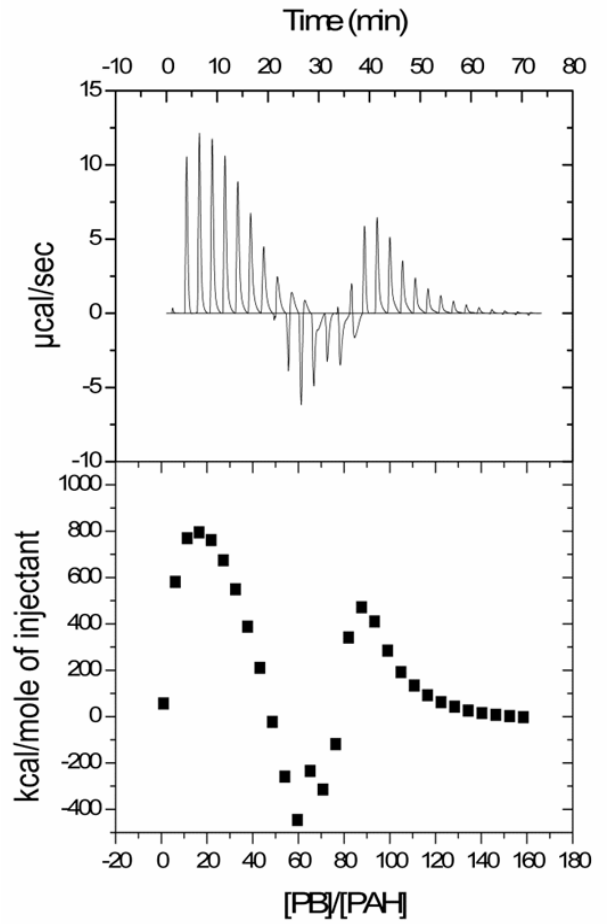

Figure 3. Isothermal titration calorimetry (ITC) curve of PANs formation. Raw data were obtained by titrating 1 mg/mL (6.7×10^{-5} M) PAH solution with 0.05 M phosphate buffer (PB) solution representing observed changes in heat resulting from interactions between polymer and phosphate shown in the upper panel. The resulting binding curve is displayed in the lower panel *vs* the molar ratio of [PB]/[PAH].

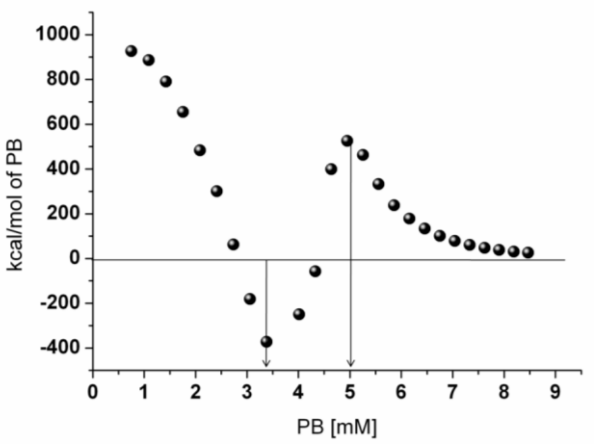

Figure 4. Isothermal titration calorimetry isotherms obtained by titrating 1 mg/mL PAH solution with 0.05 M solution of PB. Raw data have been transformed to relate the PB concentration to enthalpy changes.

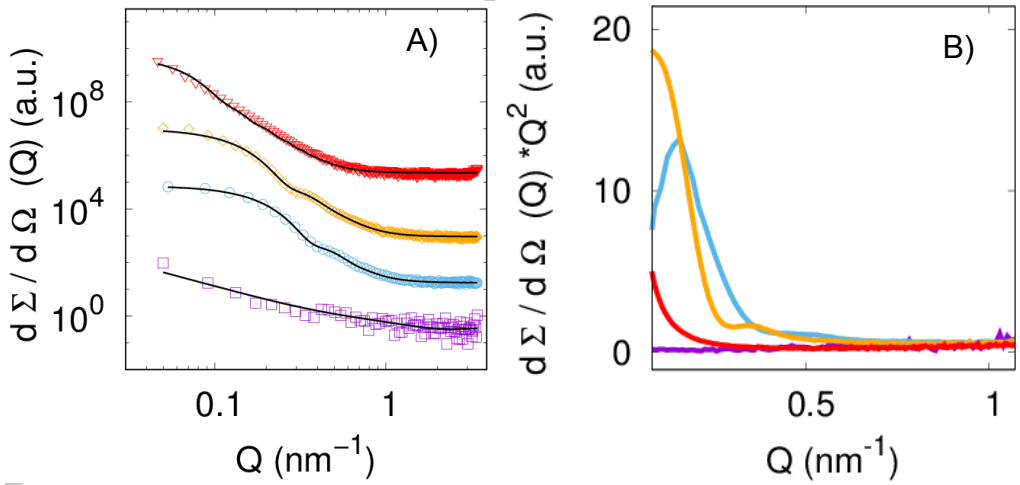

Figure 5. SAXS experimental curves of PANs formation at different PB concentration. In the Figure 5A, the SAXS experimental curves of PANs were obtained dissolving PAH at 1 mg/mL in PB at different concentrations: 1, 4, 5, and 8 mM from bottom to top); theoretical fitting are the black curves; spectra are scaled for clarity. The same SAXS curves are reported in the Kratky plot in the Figure 5B. A wider set of SAXS curves is reported in **Figure S3A**.

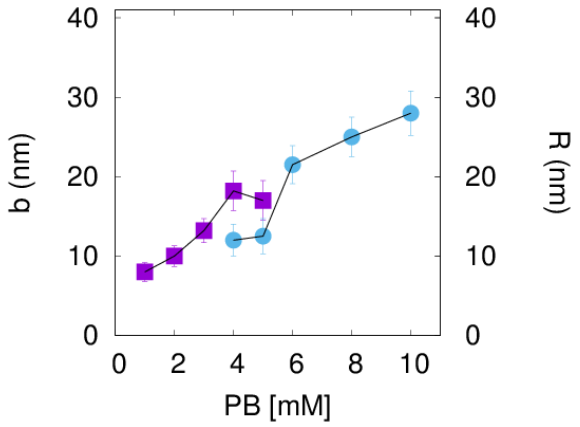

Figure 6. Structural parameters of non-complexed and complexed polymers resulting from SAXS analysis. The figure shows the variation of PANs radii ® and Kuhn length (b) for non-complexed polymers for PAH 1 mg/mL as a function of PB concentration as obtained from SAXS analysis. b (nm), refers to worm-like species (squares), and average spheres' radii, R (nm) (circles), to PANs. Lines are a guide to the eyes. Errors in fitting parameters have always been established by iteratively moving all the SAXS curve points within their experimental error, by then repeating the minimization process, and by calculating the average and the standard deviation of each fitting parameter after a number of iterations typically equal to 10.

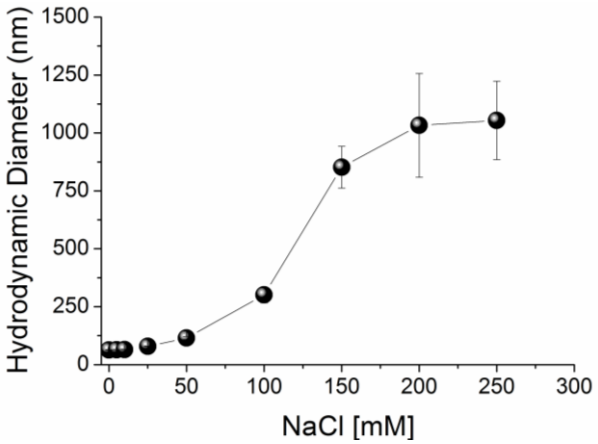

Figure 7. DLS characterization of PANs in the presence of different concentrations of NaCl. The Hydrodynamic Diameter (nm) of PANs in 5 mM PB *vs* NaCl concentration

[mM]. Results are mean of 3 independent measurements. Error bar are the standard deviation of 3 independent measurements. The lines are a guide to the eyes.

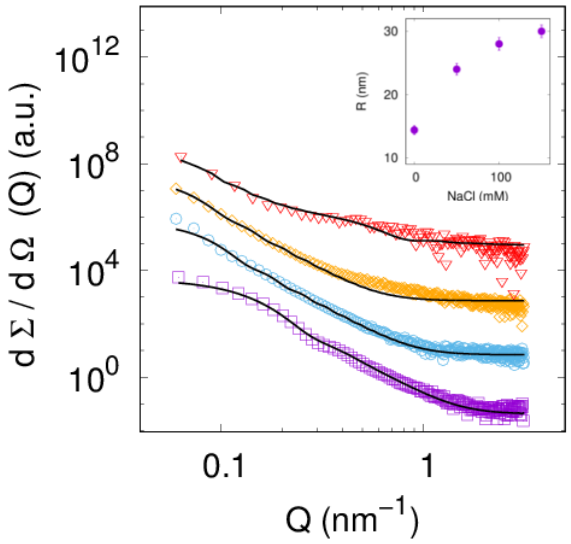

Figure 8. SAXS characterization of PANs in the presence of different concentrations of NaCl. SAXS curves, scaled for clarity, correspond to the same PB conditions and NaCl concentration increasing from bottom to top (0, 50, 100, and 150 mM). In the inset, the average radii of PANs are reported *vs* NaCl content in solution [mM].

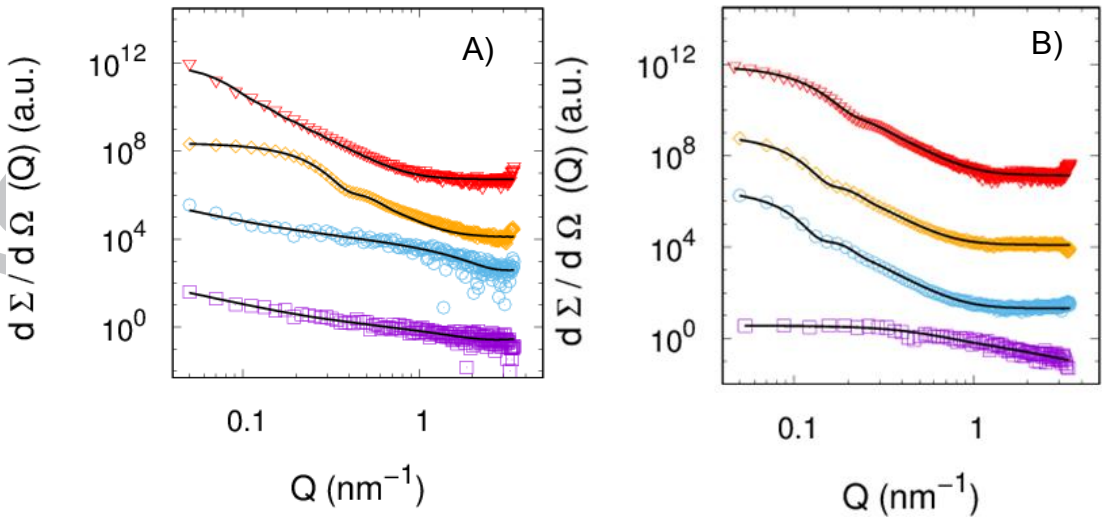

Figure 9. SAXS experimental curves and theoretical fitting as a function of the phosphate concentration for PAH exposed to a single phosphate component from PB.

A) SAXS curves are shown for 1 mg/mL PAH prepared in the presence of increasing concentrations of KH_2PO_4 (30, 45, 60, and 90 mM from bottom to top), and B) Na_2HPO_4 (2, 4, 6, and 30 mM from bottom to top). A wider set of SAXS curves is reported in **Figures S3B** and **S3C**.

REFERENCES

[1] R. Sharma, I. Zhang, T. C. Shiao, G. M. Pavan, D. Maysinger, R. Roy. Nanoscale, 8 (2016) 5106-5119.

[2] T. C. B. Klaubera, R. V. Søndergaarda, R. R. Sawant, V. P. Torchilin, T. L. Andresen. Acta Biomater. 35 (2016) 248-259.

[3] R. Kanasty, J. R. Dorkin, A. Vegas, D. Anderson. Nat. Mater. 12 (2013) 967-977.

[4] P. Andreozzi, E. Diamanti, K. Rapp Py-Daniel, P.Rocio Cáceres-Vélez, C. Martinelli, N. Politakos, A. Escobar, M. Muzio-Falconi, R. Azevedo, S. E. Moya. ACS Appl. Mater. Interfaces 9 (2017) 38242-38254.

[5] H. G. Bagariaa, and M. S. Wong. J. Mater. Chem. 21 (2011) 9454–9466.

[6] M. Chiper, N. Tounsi, R. Kole, A. Kichler, G. Zuber. J. Control Release 28 (2017) 60-70.

[7] J. Gilleron, W. Querebes, A. Zeigerer, A. Borodovsky, G. Marsico, U. Schubert, K. Manygoats, S. Seifert, C. Andree, M. Stöter, H. Epstein-Barash, L. Zhang, V. Koteliansky, K. Fiztgerald, E. Fava, M. Bickle, Y. Kalaidzidis, A. Akinc, M. Maier, M. Zerial. Nat. Nanotechnol. 31 (2013) 638-646.

[8] K. L. Kozielski, S. Y. Tzeng, B. A. Hurtado De Mendoza, J. J. Green. ACS Nano 8 (2014), 3232-3241.

[9] M. Lazebnik, D. W. Pack. J. Control Release 247 (2017) 19-27.

[10] A. V. Dobrynina, M. Rubinstein. Prog. Polym. Sci. 20 (2005) 1049-1118.

[11] H. Schiessel. Macromolecules 32 (1999) 5673-5680.

[12] H. Dautzenberg, and J. Kriz. Langmuir 19 (2003) 5204-5211.

[13] S. W. Cranford, M. J. Buehler. Macromolecules 45 (2012), 8067-8082.

[14] B. Jachimska, T. Jasiński, P. Warszyński, Z. Adamczyk. Colloids and Surfaces A: Physicochem. Eng. Aspects 355 (2010) 7-15.

[15] W. A. Marmisollé, J. Irigoyen, D. Gregurec, S. E. Moya, O. Azzaroni. Adv. Funct. Mater. 25, (2015) 4144-4152.

[16] Y. Huang, and Y. Lapitsky. J. Phys. Chem. B 117 (2013) 9548-9557.

[17] R. Georgieva, R. Dimova, G. Sukhorukov, G. Gemma Ibarz, H. Möhwald. J. Mater. Chem. 15 (2005) 4301-4310.

[18] H. Amenitsch, M. Rappolt, H. Kriechbaum, P. Mio, P. Laggner, S. Bernstorff. J. Synchrotron Rad. 5, 1998, 506-508.

[19] F. Spinozzi, C. Ferrero, M. G. Ortore, A. De Maria Antolinos, P. Mariani. J. App. Cryst. 47 (2014) 1132-1139.

[20] J. S. Pedersen, P. Schurtenberger. Macromolecules 29, (1996), 7602-7612.

[21] M. G. Ortore, F. Spinozzi, S. Vilasi, I. Sirangelo, G. Irace, A. Shukla, T. Narayanan, R. Sinibaldi, P. Mariani. Phys. Rev. E 84 (2011) 061904-10.

[22] Y. Tian, L. Li, H. Han, W. Wang, Y. Wang, Z. Ye, X. Guo. Polymers 8 (2016) 145-15.

[23] O. Glatter Fourier transformation and deconvolution in neutron, x-rays and light scattering methods applied to soft condensed matter. Eds P. Lindner & T. Zemb (2002) 103-124. Amsterdam, The Netherlands: North-Holland.

[24] M. G. Ortore, F. Spinozzi, P. Mariani, A. Paciaroni, L. R. S. Barbosa, H. Amenitsch, M. Steinhart, J. Ollivier, and D. Russo. J. R. Soc. Interface 6 (2009) S619-S634.

[25] P. G. Lawrence, and Y. Lapitsky. Langmuir 31 (2015) 1564-1574.

[26] V. S. Murthy, R. K. Rana, M. S. Wong. J. Phys. Chem. B 110 (2006) 25619-25627.

[27] C. Wang, K. C. Tam. Langmuir 18 (2002) 6484-6490.

[28] C. Wang, K. C. Tam. J. Phys. Chem. B 108 (2004) 8976-8982.

[29] O. Glatter, & O. Kratky. Small-Angle X-ray Scattering. Academic Press, London, 1982.

[30] B. Y. Ha, D. Thirumalai. Macromolecules 28 (1995) 577-581.

[31] R. Golestanian, M. Kardar, T.B. Liverpool. Phys. Rev. Lett. 82 (1999) 4456-4459.

[32] C. G. Baumann, S. B. Smith, V. A. Bloomfield, C. Bustamante. Ionic effects on the elasticity of single DNA molecules. PNAS 94 (1997) 6185-6190.

[33] J. Skolnick, and M. Fixman. Macromolecules 10 (1977) 944-948.

[34] D. J. Tobler, S. Shaw, L. G. Benning. Geochimica et Cosmochimica Acta 73 (2009) 5377-5393.

[35] H. Schiessel, and P. Pincus. Counterion-Condenstaion-Induced Collapse of Highly Charged Polyelectrolyte. Macromolecules 31 (1998) 7953-7959.

[36] S. V. Murthy, R. K. Rana, and M. S. Wong. J. Phys. Chem. B 110 (2006) 25619-25627.

[37] K. Lutz, C. Gröger, M. Sumper, and E. Brunner. Phys. Chem. Chem. Phys. 7 (2005) 2812-2815.

ASSOCIATED CONTENT

Supporting Information.

Additionally DLS data and TEM images. Additionally SAXS curve and Tables with the results obtained from SAXS curve fitting of 1 mg/mL PAH and different concentrations of PB, Na_2HPO_4, KH_2PO_4.

AUTHOR INFORMATION

Corresponding Author

*Maria Grazia Ortore

*Sergio Moya

Author Contributions

The manuscript was written through contributions of all authors. All authors have given approval to the final version of the manuscript.

ACKNOWLEDGMENT

The authors thank Elettra Synchrotron for beamtime allocation. The authors thank Central European Research Infrastructure Consortium (CERIC) for travel support, and Barbara Sartori for her technical assistance in the chemical laboratory. We also thank Dr. Julia Cope for correcting the manuscript. P. Andreozzi and S.E. Moya thanks the MAT2017-88752-R Retos project from the Ministerio de Economia, Industria y Competitividad, gobierno de España. This work was performed under the Maria de Maeztu Units of Excellence Program from the Spanish State Research Agency – Grant No. MDM-2017-0E720.

ABBREVIATIONS

DLS, Dynamic Light Scattering; ITC, Isothermal Titration Calorimetry; PAH, Poly(allylamine hydrochloride); PAN, Polyamine Phosphate Nanoparticle; PB, Phosphate Buffer; SAXS, Small Angle X-ray Scattering; TEM, Transmission Electron Microscopy.